Highly tunable heterogeneously integrated III-V on silicon sampled-grating distributed Bragg reflector lasers operating in the O-band

Hélène Duprez, C. Jany, Christian Seassal, B. Ben Bakir

Research Article | Vol. 24, No. 18 | 5 Sep 2016 | OPTICS EXPRESS 20895

Optics EXPRESS

Highly tunable heterogeneously integrated III-V on silicon sampled-grating distributed Bragg reflector lasers operating in the O-band

HELENE DUPREZ,[1,2] CHRISTOPHE JANY,[1] CHRISTIAN SEASSAL,[2] AND BADHISE BEN BAKIR[1,*]

[1]*Univ. Grenoble Alpes, CEA, LETI, MINATEC campus, CEA-Grenoble, F38054 Grenoble, France*
[2]*Univ. Lyon, Institut des Nanotechnologies de Lyon-INL, UMR CNRS 5270, CNRS, Ecole Centrale de Lyon, Ecully F-69134, France*
[*]*badhise.ben-bakir@cea.fr*

Abstract: We report on the design, fabrication and performance of the first hetero-integrated III-V on silicon sampled-grating distributed Bragg reflector lasers (SGDBR) operating in the O-band and based on direct bonding and adiabatic coupling. Two devices with different geometric parameters are presented both showing an output power in the Si waveguide as high as 7.5 mW and a continuous tuning range of 27 and 35 nm respectively with a side mode suppression ration higher than 35 dB.

OCIS codes: (250.5300) Photonic integrated circuits; (140.5960) Semiconductor lasers.

References and links

1. A. W. Fang, B. R. Koch, R. Jones, E. Lively, D. Liang, Y. Kuo, and J. E. Bowers, "A Distributed Bragg Reflector Silicon Evanescent Laser," IEEE Photonics Technol. Lett. **20**(20), 1667–1669 (2008).
2. A. Descos, C. Jany, D. Bordel, H. Duprez, G. B. de Farias, P. Brianceau, S. Menezo, and B. Ben Bakir, "Heterogeneously integrated III-V/Si distributed Bragg reflector laser with adiabatic coupling," in *39th European Conference and Exhibition on Optical Communication (ECOC 2013)*, Th.1.B.2, pp. 687 (2013).
3. C. Zhang, S. Srinivasan, Y. Tang, M. J. R. Heck, M. L. Davenport, and J. E. Bowers, "Low threshold and high speed short cavity distributed feedback hybrid silicon lasers," Opt. Express **22**(9), 10202–10209 (2014).
4. H. Duprez, A. Descos, T. Ferrotti, C. Sciancalepore, C. Jany, K. Hassan, C. Seassal, S. Menezo, and B. Ben Bakir, "1310 nm hybrid InP/InGaAsP on silicon distributed feedback laser with high side-mode suppression ratio," Opt. Express **23**(7), 8489–8497 (2015).
5. C. Sciancalepore, R. J. Lycett, J. A. Dallery, S. Pauliac, K. Hassan, J. Harduin, H. Duprez, U. Weidenmueller, D. F. G. Gallagher, S. Menezo, and B. Ben Bakir, "Low-Crosstalk Fabrication-Insensitive Echelle Grating Demultiplexers on Silicon-on-Insulator," IEEE Photonics Technol. Lett. **27**(5), 494–497 (2015).
6. K. Hassan, C. Sciancalepore, J. Harduin, T. Ferrotti, S. Menezo, and B. Ben Bakir, "Toward athermal silicon-on-insulator (de)multiplexers in the O-band," Opt. Lett. **40**(11), 2641–2644 (2015).
7. P. Bettotti, *Nanodevices for Photonics and Electronics: Advances and Applications* (Pan Stanford Publishing, 2016), Chapter 8: B. Ben Bakir, C. Sciancalepore, A. Descos, H. Duprez, D. Bordel, S. Menezo, Group III–V on Silicon: a Brand-New Optoelectronic.
8. J. C. Hulme, J. K. Doylend, and J. E. Bowers, "Widely tunable Vernier ring laser on hybrid silicon," Opt. Express **21**(17), 19718–19722 (2013).
9. A. Le Liepvre, C. Jany, A. Accard, M. Lamponi, F. Poingt, D. Make, F. Lelarge, J.-M. Fedeli, S. Messaoudene, D. Bordel, and G.-H. Duan, "Widely wavelength tunable hybrid III-V/silicon laser with 45 nm tuning range fabricated using a wafer bonding technique," in *2012 IEEE 9th International Conference on Group IV Photonics (GFP)*, 54–56 (2012).
10. M. N. Sysak, J. O. Anthes, O. Raday, J. E. Bowers, and R. Jones, "A hybrid silicon sampled grating DBR laser integrated with an electroabsorption modulator using quantum well intermixing," in *34th European Conference on Optical Communication (ECOC),* Tu.4.C.4, 1–2 (2008).
11. B. Ben Bakir, A. Descos, N. Olivier, D. Bordel, P. Grosse, E. Augendre, L. Fulbert, and J. M. Fedeli, "Electrically driven hybrid Si/III-V Fabry-Pérot lasers based on adiabatic mode transformers," Opt. Express **19**(11), 10317–10325 (2011).
12. V. Jayaraman, Z.-M. Chuang, and L. A. Coldren, "Theory, design, and performance of extended tuning range semiconductor lasers with sampled gratings," IEEE J. Quantum Electron. **29**(6), 1824–1834 (1993).
13. B. Ben Bakir, C. Sciancalepore, A. Descos, H. Duprez, D. Bordel, L. Sanchez, C. Jany, K. Hassan, P. Brianceau, V. Carron, and S. Menezo, "(Invited) Heterogeneously Integrated III-V on Silicon Lasers," ECS Trans. **64**(5), 211–223 (2014).

#263655 http://dx.doi.org/10.1364/OE.24.020895
Journal © 2016 Received 20 Apr 2016; revised 8 Jul 2016; accepted 9 Jul 2016; published 31 Aug 2016

Optics EXPRESS

14. T. Ferrotti, A. Chantre, B. Blampey, H. Duprez, F. Milesi, A. Myko, C. Sciancalepore, K. Hassan, J. Harduin, C. Baudot, S. Menezo, F. Boeuf, and B. Ben Bakir, "Power-efficient carrier-depletion SOI Mach-Zehnder modulators for 4x25Gbit/s operation in the O-band," in *Proc. SPIE, Silicon Photonics X,* 93670D 1–11 (2015).

1. Introduction

As copper interconnects and microelectronics circuits fail meeting the growing data stream demand, research has turned to fiber-based optics as a way to transfer data on a broader band and a longer reach. The price of III-V bulk optical components is however an issue and to compete with microelectronics, mass production is compulsory hence the growing interest in silicon photonics. This solution is a way to leverage the know-how acquired in processing silicon using CMOS facilities and to take advantage of the fact that Si is transparent in the C- and O-bands thus enabling to build Si waveguides at tele- and data-communication wavelengths.

However, because of its indirect bandgap, no efficient light source can be built into pure Si. Up to now, the prospect that appears the most promising in terms of design and process fabrication is to create hybrid III-V/Si laser sources where the III-V material stands for the gain region and the other functions (such as gratings or couplers) are built into the Si waveguide. Efficient III-V/Si devices have already been demonstrated including distributed Bragg reflector (DBR) lasers [1,2] or distributed feedback (DFB) lasers [3,4].

To reach broadband communication, it is necessary to transfer several wavelengths in one same waveguide (WG) using dense wavelength division multiplexing (DWDM) which can be enabled thanks to Mach-Zehnder based multiplexors, arrayed waveguide or echelle gratings [5,6]. To do so, the different laser wavelengths need to be controlled very precisely which is unrealistic if we take into consideration all the standard deviations that are inherent to fabrication processes. This is the reason why a post process wavelength control may be required for some applications. Because of their architecture, it is very tricky to tune III-V/Si DFB lasers without damaging their performances. III-V/Si DBR lasers can be tuned (as described in references [7]) but in that case, the tuning is not continuous without a phase section and the accuracy of the wavelength control does not go below the nanometer scale. Continuously tuned III-V/Si lasers were demonstrated around 1.55 µm using the Vernier effect in a double-ring cavity [8,9]. III-V/Si SGDBR lasers were also reached at 1.55 µm but the tuning was implemented using carrier injection instead of thermo-optic effect [10]. However, no continuously tuned III-V/Si lasers have ever been demonstrated in the O-band because historically, the demand for tunable devices was rather needed for telecommunication applications. Nonetheless, as the interest in datacommunication arises, the necessity to tune lasers around 1.31 µm appears as well which leads to specific design and technological challenges such as the period size decrease. This publication tackles the design, fabrication and characterization of continuously tunable hybrid III-V/Si sampled-grating DBR (SGDBR) lasers in the O-band. To our knowledge, the devices presented in this work are the first continuously tunable devices around 1.31 µm and the first III-V/Si SGDBR tuned using thermo-optic effect.

Optics EXPRESS

2. Laser architecture and design

2.1. Overall structure

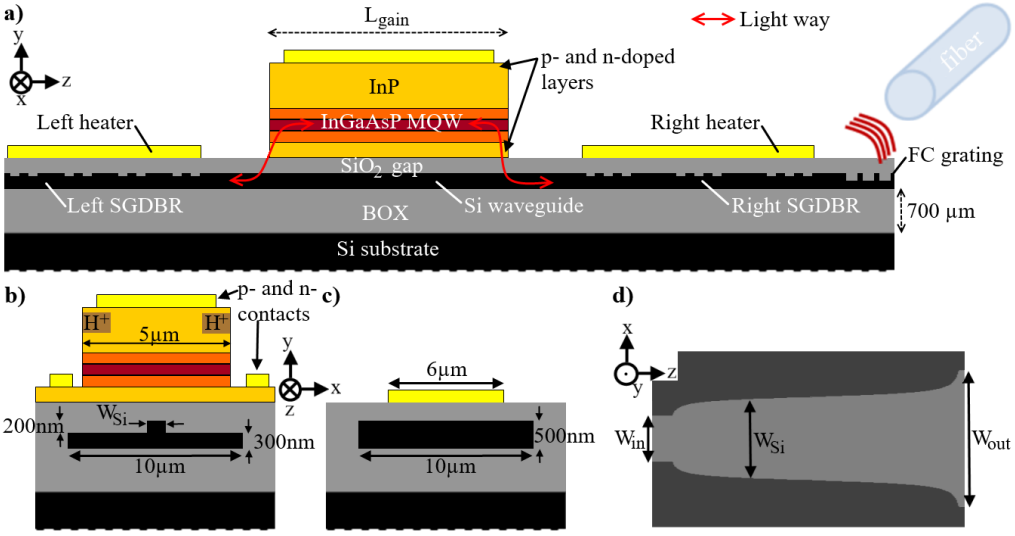

Fig. 1. (a) Schematic side view of the hybrid III-V/Si SGDBR laser (not at scale). (b) and (c) are cross sections of the laser in the active and mirror regions respectively. (d) is a top view of the III-V to silicon adiabatic coupler.

An overview of the device is displayed in Fig. 1(a). The 700-µm-long active region (L_{gain}) consists of a III-V waveguide including InGaAsP multiple QWs (MQWs), with a maximum gain centered at 1310 nm, surrounded by *p*- and *n*-doped InP layers. It stands on top of a silicon waveguide, with a SiO_2 gap of 90 nm. The laser cavity is formed by two SGDBR surrounding the active region and etched along the 500-nm-thick silicon waveguide. The red arrows schematically indicate how the light generated in the MQWs is coupled into the Si waveguide. It shows that the laser is designed, as explained below, so that light stays confined in the III-V MQWs when in the active region to maximize the gain and is transferred to the Si WG at the output of the active region.

A cross section of the gain region is represented in Fig. 1(b) showing that the Si waveguide consists of a 200-nm-thick rib on a 300-nm-thick slab. Depending on the width of the rib (W_{Si}), light is confined either in the active (III-V semiconductor) or passive (Si) WG: at both terminations of the active region, the silicon WG is widened adiabatically as in Fig. 1(d), enabling light to be coupled into the silicon with more than 90% efficiency. The principle of operation of those 100-µm-long mode transformers is fully described in [4,11] and references therein. In order to maximize the modal gain, carrier injection is concentrated in the center of the III-V active waveguide thanks to H^+ "resistive" doping on the sides of the 5-µm-wide InP/InGaAsP deep-ridge waveguide as represented in Fig. 1(b). Laser light emission is finally collected with a fiber positioned on the top of a waveguide-to-fiber surface grating coupler (FC grating).

Both mirrors are designed to reach the same reflectivity on each side of the cavity, which means that the same output power is produced at each laser output. The cross section of the SGDBR in Fig. 1(c) shows that for the mirrors, W_{Si} is as wide as the slab. To tune the device wavelength, the thermo-optics effect is used. The heater (HT) is a metallic NiFe layer deposited above each mirror; a current going through this layer heats the Si WG thanks to Joule effect. This temperature change induces a variation of the refractive indices in the mirror and a shift of its response toward higher wavelengths.

Optics EXPRESS

2.2. Sampled-grating mirror principle

The first SGDBR laser was demonstrated by V. Jayaraman et al. [12] and consisted of III-V bulk materials tuned by carrier injection. To better understand the basis of this device, a schematic view of one of the mirrors is represented in Fig. 2(a). It is based on a DBR mirror, where elementary patterns are periodically removed. Two periods are thus superimposed: 'a' the initial grating period and a_{sp} the sampling period. The reflectivity response of such a mirror is a comb for which the central wavelength depends on 'a' and the spacing between two peaks on a_{sp}. Two such responses are displayed in Fig. 2(b) for SGDBR mirrors with the same parameters i.e. a, e the etching depth and DC_{sp} the sampling period filling factor. The only difference between both mirrors is their sampling period which are respectively 29.8 µm and 26.5 µm. In both cases, their response is a comb centered on 1311 nm but the interval between their peaks is different (respectively 8 and 9 nm). Consequently, the Vernier effect results in selecting the only wavelength for which the responses are aligned: the central one as it can be seen by the R_1R_2 product (black line on the plot). Building a laser with these mirrors therefore allows for a very precise wavelength filtering thanks to this effect.

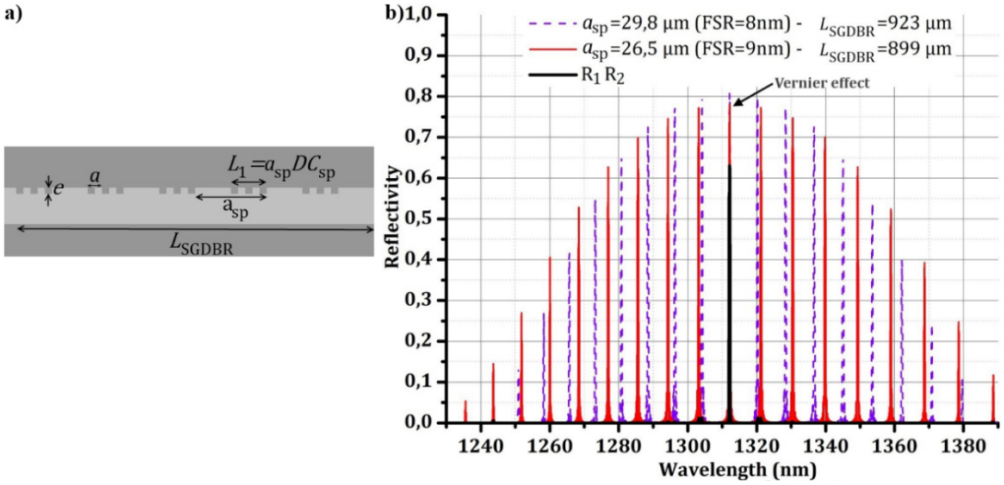

Fig. 2. (a) Schematic view of a SGDBR mirror with its different parameters. (b) Spectral responses of two SGDBR mirrors with different sampling periods. For both mirrors, a = 196 nm, e = 20 nm, DC_{sp} = 0.1 and $R_{max,SGDBR}$ = 0.8.

Regarding the tuning capability of a laser built with the mirrors from Fig. 2(b), it is clear that when heating the mirror with the highest sampling period, the peaks at longer wavelengths than the central one are successively selected. When heating the mirror with the lowest sampling period, the peaks on the left of the central wavelength are selected instead which means that this kind of cavity offers the possibility to tune the wavelength either toward lower or higher wavelengths. Using this method, the device can be tuned on a very large wavelength range, with no need for high tuning powers, but not continuously. To bridge the gap between two peaks and reach continuity, both mirrors need to be heated at the same time.

2.3. Mirror design

To design the SGDBR mirrors of the devices presented below, their responses were plotted using transfer matrix theory as well as finite element method (FEM) to calculate the effective and group indices of the modes. As represented in Fig. 2(a), the parameters to optimize when designing a SGDBR mirror are a, a_{sp}, DC_{sp}, e and L_{SGDBR}, the total grating length. The former parameter depends on the central wavelength (λ_{Bragg}) through the Bragg relation ($a = \lambda_{Bragg}/2n_{eff}$ for a first order grating where n_{eff} is the average effective index in the grating). Here, an

Optics EXPRESS

average effective index of 3.342 was calculated at λ_{Bragg} = 1310 nm using FEM, which leads to a period a = 196 nm. As for the spacing between the peaks of the comb (or its FSR for Free Spectral Range), it depends on a_{sp} and the average group index, $n_{g,avg}$ following (see [12]):

$$FSR_{SGDBR} = \frac{\lambda^2}{2n_{g,avg}a_{sp}} \quad (1)$$

Before selecting the values of the mirrors sampling periods, one has to notice that the Vernier effect occurs every:

$$\Delta\lambda_{Vernier} = \frac{FSR_{Left\ SGDBR}\,FSR_{Right\ SGDBR}}{\left|FSR_{Left\ SGDBR} - FSR_{Right\ SGDBR}\right|} \quad (2)$$

There is thus a trade-off to make between having a short gap to bridge for the continuous tuning choosing low FSR values and having a large tuning range with no second peak selected (i.e. with $\Delta\lambda_{Vernier}$ large enough so that the second peak selected stays out of reach regarding the MQWs gain). Moreover, the lower the difference between the two FSR, the higher $\Delta\lambda_{Vernier}$ but the higher the chance to get an overlap between two peaks that are not exactly aligned. For the lasers designed here, we chose not to have a difference lower than 0.5 nm between the FSR of each mirror and to get an FSR between 6 and 7.5 nm to limit the heating power while maximizing the tuning range. The sampling period values are then in the [31; 40] nm spectral range.

The mirror lengths were chosen so as to reach an 80% reflectivity for each mirror. Their values depend then on the etching depth and the sampling filling factor of the mirror. The characteristics of two SGDBR mirrors are plotted in Fig. 3 for an etching depth of either 15 nm or 25 nm. The etching depth has two effects: the lower it is, the narrower the peaks of the combs are but the longer the total grating length has to be in order to reach the same mirror reflectivity. The product of both mirror responses in Fig. 3(b) shows that from e = 25 nm, the second order peaks starts to overlap and could compete with the selected peak. To limit this overlap while working with mirrors lengths shorter than 1000 µm, e = 20 nm was selected.

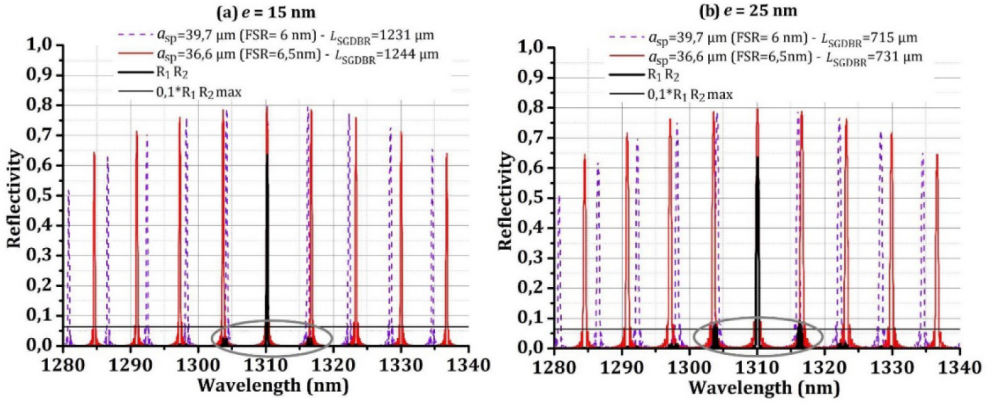

Fig. 3. Responses of two SGDBR mirrors with different FSR, a = 196 nm, DC_{sp} = 0.10 and $R_{max,SGDBR}$ = 0.8. For each plot, the etching depth is different: (a) e = 15 nm, (b) e = 25 nm. The circles highlight the other wavelengths for which the product R_1R_2 is higher than zero which might induce a competition with the central wavelength.

As it can be noticed in Fig. 4, the effect of DC_{sp} is stronger than that of e. For filling factors lower than 0.2, the lower DC_{sp}, the higher the reflectivity of higher order peaks.

Optics EXPRESS

Choosing small DC_{sp} values thus enable to reach a large tuning range. The drawback is that the total grating length needs then to be increased to reach the wanted reflectivity.

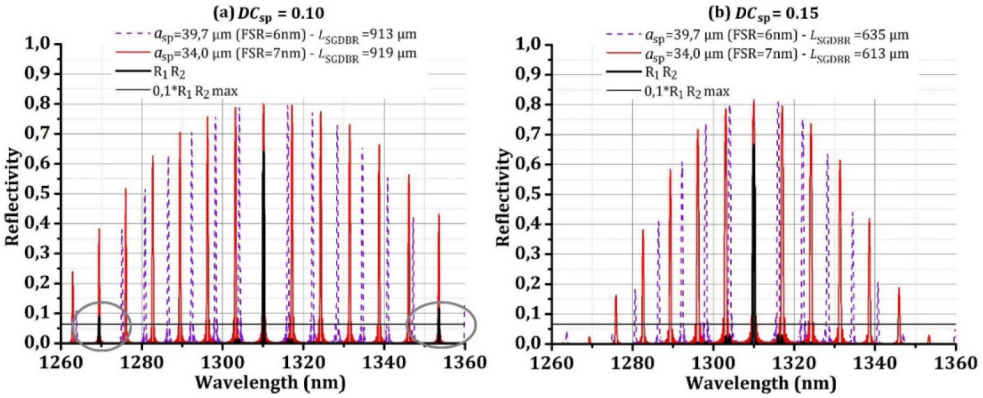

Fig. 4. Responses of two SGDBR mirrors with different FSR, a = 196 nm, e = 20 nm and $R_{max,SGDBR}$ = 0.8. For each plot, the sampling period duty cycle is different: (a) DC_{sp} = 0.10, (b) DC_{sp} = 0.15. The circles highlight the other wavelengths for which the product R_1R_2 is higher than zero which might induce a competition with the central wavelength.

However, in some cases, the second Vernier effect peak can be selected as in Fig. 4(a). For each laser design, the sampling filling factor was selected to reach the highest tuning range possible while getting rid of the second order Vernier effect.

3. Hybrid SGDBR laser fabrication

The laser fabrication process is similar to that explained in [4,13] at least until the laser pad deposition after which other steps are added for the tuning: first, a 200-mm silicon on insulator (SOI) wafer is processed with four successive lithography and reactive ion etching steps. Those include the 20-nm-deep grating level for which e-beam lithography was used to better define the grating which period is only 196 nm. This process level is followed by three others implemented using 193 nm deep UV (DUV) photolithography: the rib, the fiber-coupler grating and eventually the slab level. The SOI wafer is then encapsulated with silica and planarized by chemical-mechanical polishing (CMP) to reach a 90-nm SiO_2 thickness above the Si WG. Meanwhile, the III-V heterostructure was grown (with the same stack as the one detailed in [4]). Both wafer surfaces are then cleaned and activated to release the dangling bonds before they are put into contact. The Van der Waals bonding is then strengthen using a 3 hours annealing at 200 °C.

After the wafer bonding, the subsequent steps comprise the InP substrate removal using HCl:H_2O wet etching, the H^+ implantation and the wafer downsizing from 8 to 3 inches. The III-V waveguide is then defined by a photolithography and a CH_4-H_2 dry etching followed by the *p*- and *n*-type contact deposition and lift-off. Afterward, the 2-inches-wafer is covered by a 2-µm-thick SiN layer used for encapsulation which is opened to reach the contacts. Finally, Au metallic pads are formed. The NiFe 250-nm-thick heater metallic layer is then deposited before the Au heater pad formation.

An optical microscope picture displaying one of the devices at the end of the whole fabrication process is represented in Fig. 5 where the heater pads, the laser gain region and the fiber-coupler grating can be seen.

Optics EXPRESS

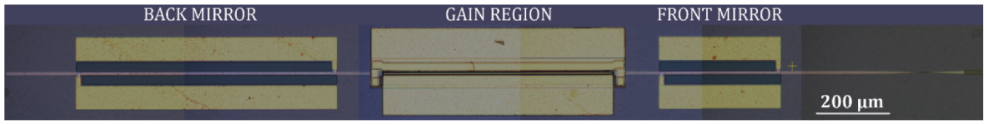

Fig. 5. Optical microscope picture of a III-V/Si SGDBR laser.

4. Experimental results

In this section, we present the results obtained for two different SGDBR lasers. Their geometrical parameters as well as the expected mirror reflectivity and FSR are gathered in Table 1

Table 1. Hybrid III-V/Si SGDBR lasers parameters.

Laser	a	L_{gain}	R	DC_{sp}	$L_{RightSGDBR}$
SGDBR 1	196 nm	700 µm	0.8	0.15	635 µm
SGDBR 2				0.10	913 µm
Laser	$a_{sp,\ RightSGDBR}$	$FSR_{RightSGDBR}$	$L_{LeftSGDBR}$	$a_{sp,\ LeftSGDBR}$	$FSR_{LeftSGDBR}$
SGDBR 1	39.7 µm	6 nm	602 µm	31.6 µm	7.5 nm
SGDBR 2			915 µm	36.6 µm	6.5 nm

The Light-power-Intensity-Voltage (LIV) curves corresponding to these devices are plotted in Fig. 6. We can first notice that the resistance is quite high: a linear fit made on the voltage versus current leads to resistances of 22 and 51 Ω for SGDBR lasers 1 and 2 respectively. These high values are attributed to the fact that during process, the MQWs were too deeply etched and the n-doped InP layer is consequently not thick enough to get proper laser resistances: respectively 125 nm and 100 nm instead of the 150 nm wanted. This also explains the high threshold current values. In spite of this problem and because SGDBR cavities have high quality factors, the devices presented below display high output powers. After removing the insertion losses into the fibers, measured to be 6 dB, the output power of both laser reaches 7.5 mW within the Si WG (taking into account both sides of the laser since as much power is produced on the left as on the right output). The kinks of the LI curve are due to mode hops which are unavoidable with such a laser architecture: as carriers are injected into the cavity, a thermal detuning occurs within the gain region and the Vernier effect occurs on another peak.

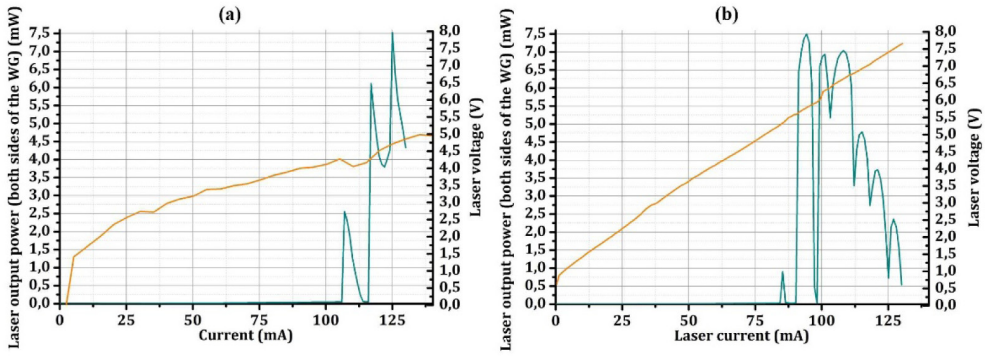

Fig. 6. Laser output power (taking into account both laser outputs) and voltage as a function of the laser injection current for two different SGDBR lasers (laser 1 and 2).

Spectra measured for laser SGDBR 1 are displayed in Fig. 7 for different heater currents injected, showing in each case a side mode suppression ration (SMSR) higher than 40 dB. These graphs give a good overview on how the tuning takes place: the peaks corresponding to each mirror are clearly distinguishable with those related to the right SGDBR below, and

Optics EXPRESS

to the left SGDBR above the background curve. As one of the mirrors is heated, either the peaks below or above are shifted toward higher wavelengths and another wavelength is selected.

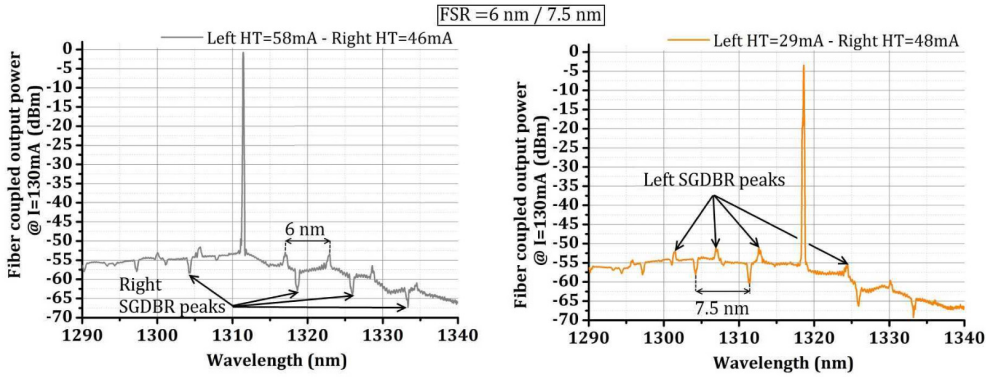

Fig. 7. Spectra, at different heaters injection currents, for SGDBR 1 (FSR_{left} = 6 nm / FSR_{right} = 7.5 nm).

The peak wavelength reached by the lasers depending on both their left and right heater powers is given in Fig. 8. Both lasers show continuous tuning over a 27 and 35 nm range for SGDBR laser 1 and 2 respectively. On the whole tuning range, the SMSR belongs to the [35; 50] dB range and the power fluctuates between 1 and 8 mW in both cases. It is important to notice that here, the laser injection current was set to either 130 mA or 120 mA respectively and only the heaters injection currents were modified. To get less power fluctuations, the laser injection current shall be adjusted or a phase section might be added.

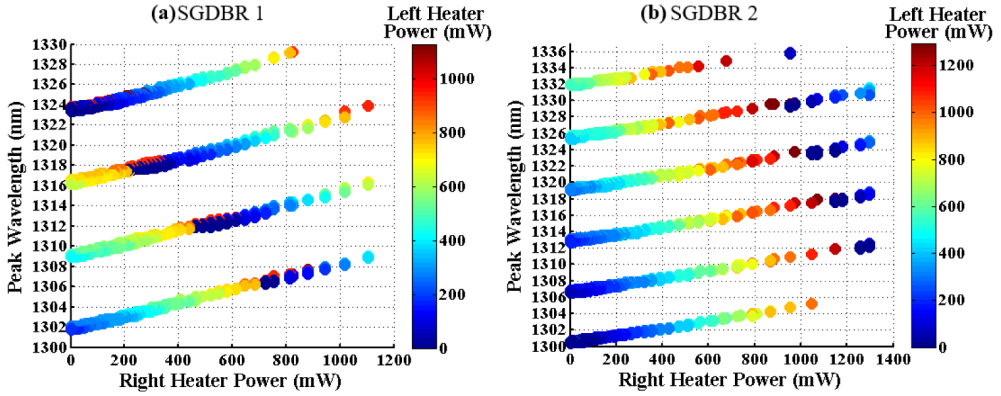

Fig. 8. Peak wavelength depending on the power of both heaters for SGDBR 1 at I = 130 mA (a) and SGDBR 2 at I = 120 mA (b).

For the former device, the heater powers reach 900 mW for the left one and 1100 mW for the right one to sweep along the whole wavelength range. For the SGDBR laser 2, heater powers of rather 1300 mW are needed because the mirrors are longer (see Table 1) and thus have higher resistances. Consequently, the power needed to reach the same temperature difference (and index change) is higher for the second laser. The advantage of the SGDBR laser 2 is that the FSR of the right mirror is 6.5 nm compared to 7.5 nm for the first laser. It is therefore easier to select more peaks and thus reach a higher wavelength range.

Spectra measured from the SGDBR laser 1 equally spaced by 0.8 nm are displayed in Fig. 9. It shows that with such a device, it is possible to control very precisely the wavelength of interest and that this device could be used for DWDM applications. The laser injection

Optics EXPRESS

current is set to 130 mA and only the heater powers are modified. To obtain the same power for all the wavelength (which is not the case here), measurements including laser injection current changes should be implemented.

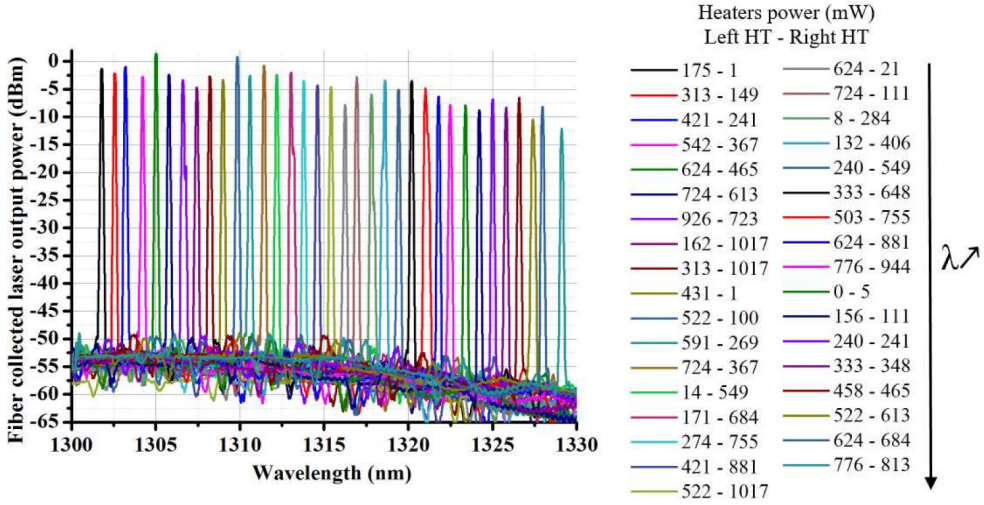

Fig. 9. Spectra of SGDBR 1 at different heaters power values for a 130 nm laser injection current. Each spectrum is separated from the following one by a 0.8 nm interval.

5. Conclusion

We have reported on the demonstration of the first widely-tunable hybrid III-V/Si SGDBR lasers operating in the O-band. Through the study of two lasers with different opto-geometrical parameters we could conclude that a shorter sampling filling factor for the mirror induces the need for more tuning power. We also showed that a smaller size difference between the sampling period of each mirror within the cavity enables to select more peaks within the gain region and thus get a device tunable on a wider range.

An output power as high as 7.5 mW in the Si waveguide was demonstrated and most importantly a continuous tuning range of 35 nm was reached. The lasers are single-mode on the whole spectral range and exhibit a SMSR higher than 35 dB. This wavelength range thus correspond to ± 1.34% of the 1.31 µm central wavelength. This is close to the state of the art value of ± 1.45% reached at 1.55 µm in [9] with a double-ring based architecture.

Current and future works are mostly focused on improving the heater efficiency to limit the tuning power consumption, lowering the contact resistance and building lasers with wider spectral-gain responses to achieve a broader wavelength tunability. To provide high volume, low-cost and compact solutions for (400G and beyond) next-generation optical interconnects, the wafer-level co-integration of such hybrid III-V/Si lasers with modulators [14], multiplexors, photodetectors and their electronic IC's is currently in progress.

Acknowledgments

The authors would like to thank K. Hassan for the discussions on thermal effect as well as K. Ribaud and P. Grosse for their help on device characterization. This work was supported by the French national program *'programme d'Investissements d'Avenir'*, IRT Nanoelec, Grant ANR-10-AIRT-05.